Available online at www.sciencedirect.com
SCIENCE DIRECT®
Journal of Nuclear Materials 337–339 (2005) 766–770
journal of nuclear materials
www.elsevier.com/locate/jnucmat

Erosion of tungsten armor after multiple intense transient events in ITER

B.N. Bazylev [a,*], G. Janeschitz [b], I.S. Landman [a], S.E. Pestchanyi [a]

[a] Forschungszentrum Karlsruhe, IHM, P.O. Box 3640, 76021 Karlsruhe, Germany
[b] Forschungszentrum Karlsruhe, Fusion, P.O. Box 3640, 76021 Karlsruhe, Germany

Abstract

Macroscopic erosion by melt motion is the dominating damage mechanism for tungsten armour under high-heat loads with energy deposition $W > 1\,\mathrm{MJ/m^2}$ and $\tau > 0.1\,\mathrm{ms}$. For ITER divertor armour the results of a fluid dynamics simulation of the melt motion erosion after repetitive stochastically varying plasma heat loads of consecutive disruptions interspaced by ELMs are presented. The heat loads for particular single transient events are numerically simulated using the two-dimensional MHD code FOREV-2D. The whole melt motion is calculated by the fluid dynamics code MEMOS-1.5D. In addition for the ITER dome melt motion erosion of tungsten armour caused by the lateral radiation impact from the plasma shield at the disruption and ELM heat loads is estimated.

PACS: 52.40.Hf
Keywords: Plasma–material-interection; Erosion; Divertor; ELMs

1. Introduction

Tungsten is foreseen as one of the ITER armor materials for the divertor and the dome. For the strongest transient events (TE) such as disruptions, the most important mechanisms of metallic armour damage are surface melting and melt splashing [1,2]. During ITER operation expected total number of disruptions may reach several hundred. Operation in the Type I ELMy H-mode with about 10^3 ELMs per discharge is assumed as the reference ITER regime [3]. ELMs have much smaller impact on armour. However in ITER ELM energies may also exceed the melting threshold [4] and thus the melt motion erosion becomes the main mechanism of armour damage.

The numerical analysis [2] for tungsten armour damage demonstrated that in case of a single disruption with the energy deposition $W > 30\,\mathrm{MJ/m^2}$ and the time scale $\tau \sim 10\,\mathrm{ms}$ the crater depth caused by the melt motion may reach up to $10^2\,\mu\mathrm{m}$, which is drastically distinct from the single ELM damage where the surface roughness about $1\,\mu\mathrm{m}$ was obtained for $W = 3.5\,\mathrm{MJ/m^2}$ and the time scale $\tau = 0.5\,\mathrm{ms}$. At the multiple ELM loads for the ITER conditions under the assumption of stochastic motion of the separatrix strike position (SSP) along the divertor surface the erosion rate essentially decreases, compared to the case with fixed SSP, and at the ELM number larger than 10^3 evaporation becomes to be the main erosion mechanism [5]. During ITER operation, several thousand ELMs can be expected between

* Corresponding author. Tel.: +49 07247 825987; fax: +49 07247 824874.
E-mail address: bazylev@ihm.fzk.de (B.N. Bazylev).

0022-3115/$ - see front matter © 2004 Elsevier B.V. All rights reserved.
doi:10.1016/j.jnucmat.2004.10.070

disruptions. For a realistic estimation of the tolerable number of such events, the consequence of such combined load of sequential disruption and multiple ELMs has to be simulated.

The heat loads typical of single giant ELMs and disruptions produce an ionized plasma shield in front of the target [6]. The shielding layer consists of material atoms and is a source of intensive radiation of GW/m^2 level. The radiation exposes the surface of the dome elements nearby, which may cause its melting, evaporation, formation of its own plasma shield and further damage due to the melt motion. The energy threshold of intense transient events for the dome damage should be also estimated.

In this work the influence of melt motion on the damage to tungsten of the divertor armour at the repetitive disruption loads interspaced by multiple ELMs is numerically investigated for the ITER conditions. The magnitude of roughness after many transient events with the heat loads stochastically distributed over the divertor surface is simulated applying the quasi-one-dimensional fluid dynamics code MEMOS-15.D described in [1]. For multiple transient events the dependence of surface roughness on the dispersion of stochastic motion of SSP is analyzed. For different single transient events the erosion of the dome elements caused by the radiation from the plasma shield is estimated. The time dependent spatial profiles of impacting heat fluxes and plasma pressure at the target surface are calculated with the radiation MHD code FOREV-2D [6] taking into account the shielding effect and the lateral radiation from the plasma shield.

2. Simulation implications

Almost at all tokamaks the heat flux profiles of Type I ELMs have a pronounced peak near SSP both for the inner- and outer divertor legs [7,8] and acquire rather complicated patterns at the armour plates [7]. High-speed measurements indicate a fast temperature increase at the divertor surface during ELMs, of 0.1 ms (JET), 0.3 ms (DIII-D), and 0.3 ms (AUG) followed by a rather long temperature drop, that can exceed 1 ms [9]. However, the whole duration of ELM power deposition as well as its time dependence is not known sufficiently.

Experimental data on stochastic behavior of the disruption loads are not available. Nevertheless from the experimental data obtained with various diagnostics at JET, AUG and DIII-D for sequential ELMs, a stochastic behavior of the heat flux magnitude as well as SSP can be concluded [7–12]. It is assumed that the position of SSP at the divertor plate stochastically changes from one transient event to another, having a Gaussian distribution with the dispersion ranging from 0.05 and 0.1 m and a scanning width of 0.2 m. For multiple events the total erosion is considered to be the sum of the erosions of the sequential transient events with the stochastically varied position of SSP at the divertor plate. Influence of hot spots on the surface heating is not analyzed. For distinction below it is assumed that one disruption occurs after more than 10^3 ELMs. In the simulation for ELMs the peak of W at SSP ranges as W_{ELM} = 1–6 MJ/m^2, and Δt_{ELM} = 0.2–0.5 ms [5]. For disruptions, two scenarios are simulated: one (scenario A) with the SSP heat load W_D = 150 MJ/m^2 and Δt_D = 5 ms and another (B) W_D = 30 MJ/m^2 and Δt_D = 10 ms. An exponential drop of power deposition in the SOL from separatrix in perpendicular midplane cross section with the half width of 5 cm is assumed. At the inclination angle of the vertical target of 20° the wetted area of vertical divertor of 30–50 cm then follows. For disruptions, profiles of heat loads and plasma pressure are analogous to that given in Ref. [5] for the ELM with W_{ELM} = 3.5 MJ/m^2 and t_{ELM} = 0.5 ms. The influence of the Lorentz force on the melt motion is investigated by varying the current through the target in the range from 0.5 to 2 MA/m^2 (as can be concluded from Ref. [13]). The directions of magnetic field and the current are chosen to result in the Lorentz force generating a downstream melt motion.

The melt motion in the code MEMOS-1.5D is described in the 'shallow water' approximation [1], with the surface tension, viscosity of molten metal, and the radiative losses from the hot surface taken into account. The plasma pressure gradients along the divertor plate, as well as the gradient of surface tension and the Lorentz force of the currents crossing the melt layer immersed in strong magnetic field, produce the melt acceleration. A two-dimensional heat transport equation with two boundary conditions at the moving vapor–liquid- and liquid–solid interfaces describes the temperature inside the target. Temperature dependent thermophysical data are used [14].

3. Erosion of divertor armour after repetitive ELMs

Simulations of the divertor armour damage under single ELMs demonstrated that for all scenarios the depth of melt pool is always below 80 μm and it resolidifies after the end of ELM within 2–2.5 ms, due mainly to radiation losses [5]. The single ELMs with W_{ELM} from 1 to 2 MJ/m^2 produce melting without evaporation and surface roughness after resolidification is a small fraction of micron, due to the melt motion with the melt velocity V less than 0.3 m/s caused by the Lorentz force. At W_{ELM} > 2.5 MJ/m^2 the vapor shield forms and thus the pressure gradient becomes essential. The magnitude of surface roughness is of 0.3–0.5 μm, V of 0.5 m/s, and the evaporation thickness of 0.13 μm, as demonstrated in Fig. 1(a). The Lorenz force intensifies the melt motion. The melt velocity increases up to 0.8 m/s and the

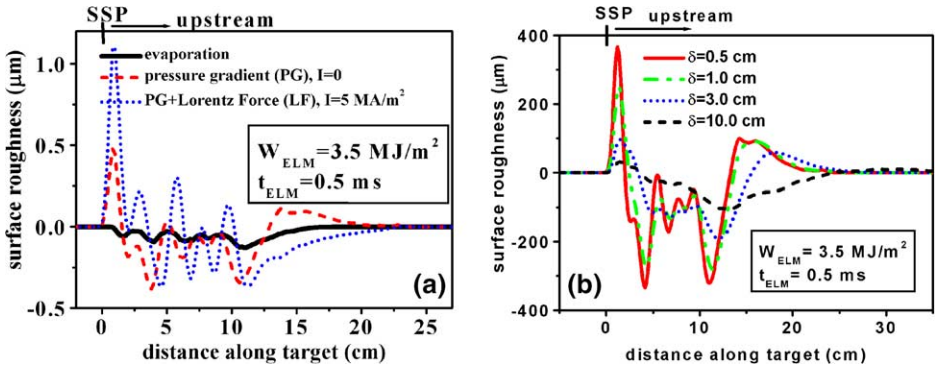

Fig. 1. Surface roughness (a) for single ELM with and without currents, (b) after 10^3 ELMs for the SSP Gaussian distribution with different δ.

surface roughness up to 1.1 m, with the crater depth less than 0.5 μm. The typical half-width of the surface roughness produced during ELMs is 0.01–0.02 m (Fig. 1(a)).

The shielding layer formed above the divertor for ELMs with 2.5 MJ/m^2 < W_{ELM} < 4 MJ/m^2 is the source of the intensive radiation load at the dome surface facing the divertor, which ranges between 1 and 3 GW/m^2 with the width of irradiated area of 0.2–0.3 m. This irradiation does not cause melting of the tungsten armour, because of its rather short time duration of 0.2–0.3 ms. For ELMs with W_{ELM} > 4 MJ/m^2, melting of dome surface occurs with depth of melt pool of 30–40 μm.

The profiles of surface roughness after 10^3 ELMs are shown in Fig. 1(b) for W_{ELM} = 3.5 MJ/m^2 and Δt_{ELM} = 0.5 ms for different scenarios of SSP motion. At fixed SSP (δ = 0.5 cm), the crater depth produced by the melt motion reaches 320 μm with mountain magnitude of 370 μm at the crater edge. The stochastic motion of SSP results in a decrease of the crater depth (see Figs. 1(a) and 2). When the dispersion δ exceeds twice the typical half-width of the surface roughness (δ > 3 cm), this effect becomes significant: the crater depth becomes less then 200 μm and drops down to 105 μm for δ = 10 cm. Further increase of δ up to 20 cm leads to the further modest decrease of the crater depth. The magnitude of the mountains at the crater edges drops more quickly (Fig. 2).

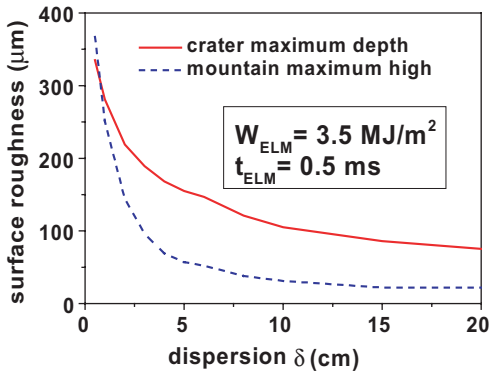

Fig. 2. Maximum magnitude of surface roughness after 10^3 ELMs versus the SSP Gaussian dispersion δ.

4. Erosion of tungsten armour after disruptions and repetitive ELMs

Two mentioned scenarios for single disruptions (A and B) are modeled. Simulations demonstrated that for both scenarios the depth of melt pool is always below 400 μm and it resolidifies within 10–12 ms, due mainly to radiative cooling. The distinguishing feature of disruption is that melted area significantly increases (up to 20 cm in the upstream direction) due to re-radiation from the expanding plasma shield. The pressure gradient generates violent melt motion with the velocities of 1–2 m/s in both directions from the maximum of pressure profile. The Lorenz force intensifies the melt motion and may change its direction to preferentially downstream. The total magnitude of surface roughness after resolidification is about 30 μm for scenario A and about 70 m for scenario B with long disruption duration (10 ms), as shown in Fig. 3. Moreover, in the first case, mountains are formed at the distance of about 10 cm from SSP and eroded area significantly increases. At rather large currents the asymmetric profile of the erosion is formed with the mountain in the downstream direction. Simulations demonstrated that the width of the eroded area increases up to 0.2–0.4 m being proportional to the half width of the pressure profile. The depth of erosion crater is proportional to the duration of heat load.

The well-developed shielding layer formed above the divertor for all types of the disruptions is an intensive source of radiation at the dome surface. The radiation flux at the dome surface may reach 2–7 GW/m^2 during

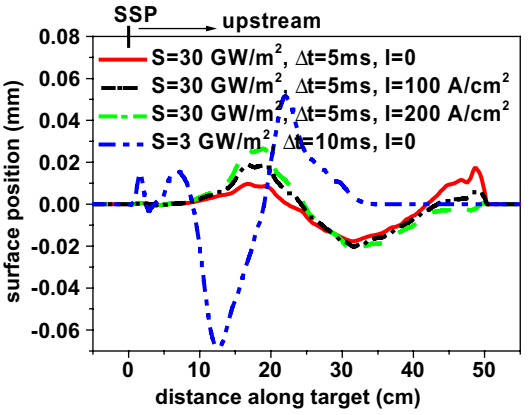

Fig. 3. Single disruption surface roughness with and without currents for two scenarios.

several ms with a width of most irradiated area of 0.3–0.5 m. The intensive radiation causes melting up to depth of 200–300 μm and its power at the dome surface is high enough to evaporate amount of the tungsten sufficient for formation of a rather thick secondary shielding layer near the dome surface, with the plasma pressure and the radiation flux comparable with that at the divertor surface. Thus it is expected that the melt motion has to be also responsible for the erosion of the dome elements.

Numerical simulation for the consequences of multiple disruptions interspaced by ELMs is based on the erosion additivity for multiple events, applied as sequential ELMs [5]. Fig. 4(a) demonstrates dependence of maximum crater depth on W_{ELM} for the cases of SSP motion with a Gaussian distribution and $\delta = 0.1$ m. Both scenarios in which each disruption is accompanied by 10^3 ELMs are compared with the case of ELMs only. The error bars indicate variations of roughness due to the currents of 5 MA/m^2. The simulations showed that for ELMs with $W_{ELM} > 2.5$ MJ/m^2 (well-developed shielding layer) the damage produced by disruptions is negligible in comparison with that produced by 10^3 ELMs and only for the weak ELMs ($W_{ELM} < 2$ MJ/m^2) disruptions may play dominant role in the armour damage. Fig. 4(b) demonstrates decreasing influence of the disruptions on the total armour erosion after 10^4 weak ELMs and the practically linear dependence of crater depth on the number of ELMs after about 10^3 ELMs.

5. Summary

The MEMOS simulations demonstrated that for disruptions and giant ELMs with $W_{ELM} > 2.5$ MJ/m^2 the pressure gradient of the plasma shield is mainly responsible for intensive melt motion at the surface of tungsten target. The melt velocities of 1–2 m/s and the surface roughness of 1 μm for ELMs are obtained. For disruptions the roughness increases up to 70 μm. For the ELMs without the vapor shield ($W_{ELM} < 2$ MJ/m^2) only the Lorentz force can generate the melt motion, with the velocities less than 0.3 m/s and surface roughness that is a small fraction of micron.

The assumption about the stochastic motion of SSP along the target surface results in essentially decreased total erosion compared with fixed SSP. This effect becomes significant as soon as the dispersion of stochastic motion exceeds twice the typical half-width of the surface roughness produced by single transient events.

The lifetime of divertor armour is determined by the melt motion produced during ELMs. If total number of weak ELMs exceeds 10^4, the erosion produced due to the disruptions is negligible in comparison with that due to ELMs even with one disruption per 10^3 ELMs. For the giant ELMs this is true when the number of ELMs is less then 10^3.

For all types of disruptions the plasma shield formed above the divertor armour generates intense radiation at the dome surface facing the divertor, which may reach a magnitude of 2–7 Gw/m^2 during several ms with the width of the highly irradiated area of 0.3–0.5 m. The radiation causes melting, evaporation of irradiated sur-

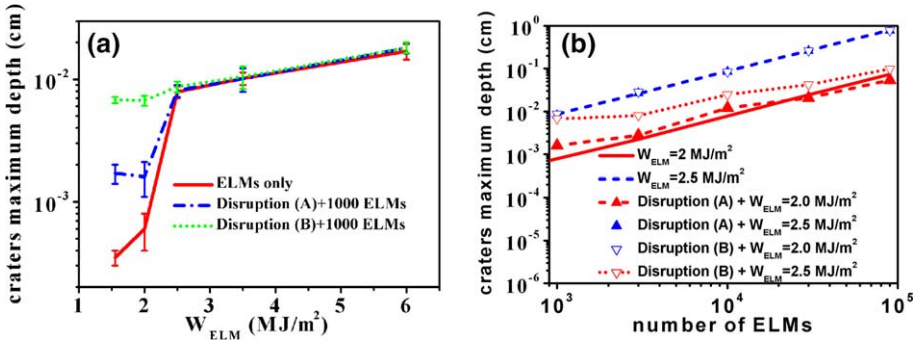

Fig. 4. (a) Crater maximum depth after combination 1 disruption and 10^3 ELMs, $\delta = 0.1$ m. (b) Crater maximum depth versus ELM number for the same conditions.

faces, and formation of a plasma shield layer that may lead to erosion of dome armour comparable with the final erosion of the divertor plate. ELMs do not cause the erosion of dome armour because of a rather weak plasma shield.

To check these results systematic experiments on tungsten erosion under repetitive pulsed plasma stream loads of 1–3 MJ/m^2 and pulse duration of 0.1–0.5 ms are necessary.

Acknowledgement

The work was performed under EFDA contract TW3-TPP-DISELM.

References

[1] B. Bazylev, H. Wuerz, J. Nucl. Mater. 307–311 (2002) 69.
[2] H. Wuerz et al., J. Nucl. Mater. 307–311 (2002) 60.
[3] ITER Physics Basis, Nucl. Fusion 39 (1999) 2137.
[4] G. Janeshitz, J. Nucl. Mater. 290–293 (2001) 1.
[5] B. Bazylev et al., Europhys. Conf. Abstr., vol. 27A (2003) P-2.44.
[6] H. Wuerz et al., J. Nucl. Mater. 290–293 (2001) 1138.
[7] A. Hermann et al., J. Nucl. Mater. 313–316 (2003) 759.
[8] N. Asakura et al., Plasma Phys. Control. Fusion 44 (2002) A313.
[9] A.W. Leonard et al., J. Nucl. Mater. 266–269 (1999) 109.
[10] G. Federici et al., J. Nucl. Mater. 313–316 (2003) 11.
[11] A. Loarte et al., Plasma Phys. Control. Fusion 44 (2002) 1815.
[12] E.R. Solano et al., Europhys. Conf. Abstr., 27A (2003) P-1.106.
[13] J. Lingertat et al., J. Nucl. Mater. 241–243 (1997) 402.
[14] Y.S. Touloukian (Ed.), Thermophysical Properties of Materials, Macmillan, New York, 1970.